ISSN 1 746-7233, England, UK
World Journal of Modelling and Simulation
Vol. 7 (2011) No. 3, pp. 173-188

Consistent bond graph modelling of planar multibody systems

Tarun Kumar Bera , Arun Kumar Samantaray*

Department of Mechanical Engineering, Indian Institute of Technology, Kharagpur 721302, India

(*Received February 14 2010, Accepted February 1 2011*)

Abstract. Modelling of mechanisms is not a trivial task because the goal is not only to obtain consistent kinematics but also to get proper dynamic loads. Therefore, a modular modelling approach is preferred for large and complex mechanisms. This paper discusses modular bond graph modelling of planar mechanical systems composed of rigid bodies, which are constrained together through a set of joints. Bond graph models of revolute joints with clearance and/or flexibility and mass distribution in prismatic or slider joints are developed. Bond graph models obtained from hierarchical composition of subsystem models are then used to calculate the dynamic loads. Two separate mechanisms are considered as illustrative examples and their bond graph models are validated through numerical simulations.

Keywords: bond graph, multibody systems, rigid body mechanics, mechanisms

1 Introduction

Multibody systems consist of rigid and elastic bodies, various types of joint components[16], passive and active coupling elements. Large transient dynamic forces are often setup in multibody systems, e.g. a telescopic rotary crane having a boom of elastic structure[20], and they are so often incorrectly neglected in the design stage due to improper modelling. These dynamic forces can be determined by simulation of a properly developed model of the actual system or by experimentation. The first step in the dynamic analysis of a mutibody system is the modelling of its components. In this article, we consider planar mechanisms with closed kinematic loops. While simple mass lumping methods provide compact models, they often give incorrect dynamic forces due to incorrect representation of inertias and constraint forces. On the other hand, variational mass lumping method becomes too cumbersome when the mass distribution is time varying. The objective of this work is to develop hierarchically composable sub-models for elements of closed loop planar mechanisms which can be composed in different ways to assemble different forms of mechanisms while automatically taking care of the kinematic, dynamic and energetic consistency of the resultant model. By adopting the bond graph modelling formalism[3, 4, 9, 12, 18, 25], the concept of causality comes handy in segregating the sub-models, defining their composition architecture and ensuring the model consistency.

The equations of motion of a multibody system can be analyzed in different ways based on the principle used (Newton-Euler method, Principle of virtual work, Principle of virtual power etc.), coordinating system used (Cartesian and Lagrangian coordinating systems), and the kinematic constraints of the system (Coordinate portioning method and augmented Lagrange formulation)[8]. The dynamic equations for the multibody systems may be expressed by Jourdain's principle and the Lagrange multiplier method together with Baumgarte's stabilization[2, 15]. The number of equations increases when Lagrange multipliers are used. Moreover, when there is a little change in the configuration, the afore-mentioned process has to be repeated again, i.e., the derivation process is not in a modular algorithmic form. Modular approach [13] is essential when designing or analyzing large/complex mechanisms. Linear graph theoretic approach[17] has been shown to be a good way of modular representation of multibody system dynamics. Karnopp and Margolis [11] developed a systematic

* Corresponding author. Tel.: +91 3222 282998/282999, fax: +91 322228227. *E-mail address*: samantaray@lycos.com.

approach to modelling of planar mechanisms by using bond graphs[3, 4, 9, 12, 18, 25]. The bond graph formalism allows us to systematically organize large number of equations. Moreover, when the user modifies the model, the equations of motion are systematically derived from the revised model. Dymola [19] is an object oriented modelling language, which provides a modular approach to model large interconnected systems. Various other object oriented bond graph software tools are also available commercially. Moreover, bond graph models are easily portioned by breaking bonds and introducing interface ports. Partitioning of models and use of separate simulation software tailored for specific subsystems have been explored recently in the context of multibody system simulation in reference[22].

To start with, we develop the bond graph model rigid planar links. Thereafter, we consider modelling of flexible joints and the impact forces at flexible joints with clearance. Then the model of a slider element with proper representation of contact forces is developed. Although simple kinematic relations are used to construct this bond graph model, the model by itself takes care of Coriolis and centrifugal forces due to the inherent power conservative properties of bond graph. This model shows the modularity of bond graph modelling in dealing with complex mechanisms. Finally, we consider two case studies: a Rapson slide and a seven-body mechanism[24]. The simulation results from these two models are compared with those obtained through other means and the results available in the literature.

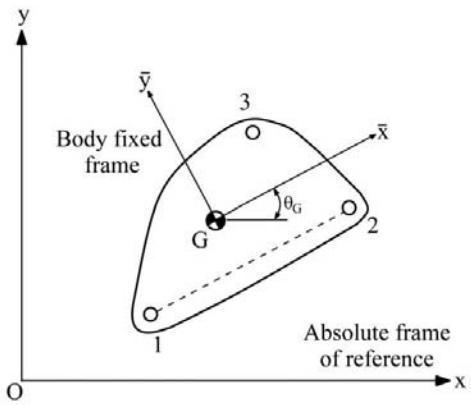

Fig. 1. Schema for a three-port rigid link

2 Modelling of planar mechanisms

2.1 Model of rigid planar links

We use a body fixed frame $\bar{x} - \bar{y}$ on a rigid link and relate the motions to the absolute frame of reference $x - y$ through appropriate velocity transformation. The displacements of any point (i^{th} point) on the rigid link, as shown in Fig. 1, are expressed in terms of linear displacements (x_G, y_G) of the center of gravity in the $x - y$ plane and angular position (θ_G) of the center of gravity about the z-axis as follows:

$$\begin{bmatrix} x_i \\ y_i \end{bmatrix} = \begin{bmatrix} x_G \\ y_G \end{bmatrix} + \begin{bmatrix} \cos\theta_G & -\sin\theta_G \\ \sin\theta_G & -\cos\theta_G \end{bmatrix} \begin{bmatrix} \bar{x}_i \\ \bar{y}_i \end{bmatrix}, \tag{1}$$

where $\bar{x}_i$ and $\bar{y}_i$ define the position of a point in the body-fixed frame. Differentiating Eq. (1) with respect to time, and noting that and are constant in a rigid body, one obtains

$$\dot{x}_i = \dot{x}_G + \mu_{x_i}\dot{\theta}_G, \tag{2}$$

$$\dot{y}_i = \dot{y}_G + \mu_{y_i}\dot{\theta}_G, \tag{3}$$

where $\mu_{x_i} = -(\bar{x}_i \sin\theta_G + \bar{y}_i \cos\theta_G)$ and $\mu_{y_i} = \bar{x}_i \cos\theta_G - \bar{y}_i \sin\theta_G$.

Eqs. (2) and (3) are sufficient to construct the augmented bond graph model of the rigid link as shown in Fig. 2. We have considered a rigid link with three joints, but the model may be extended to connect to any number of body components by joint components[17]. In Fig. 2, the mass and rotary inertia are modelled by I-elements connected to the 1-junctions representing the velocities of the center of gravity in the inertial frame. In the bond graph model given in Fig. 2, a bond with a circle over it represents a vector bond and a thick vertical line is used to split a vector bond into scalar bonds or to merge scalar bonds to form a vector bond.

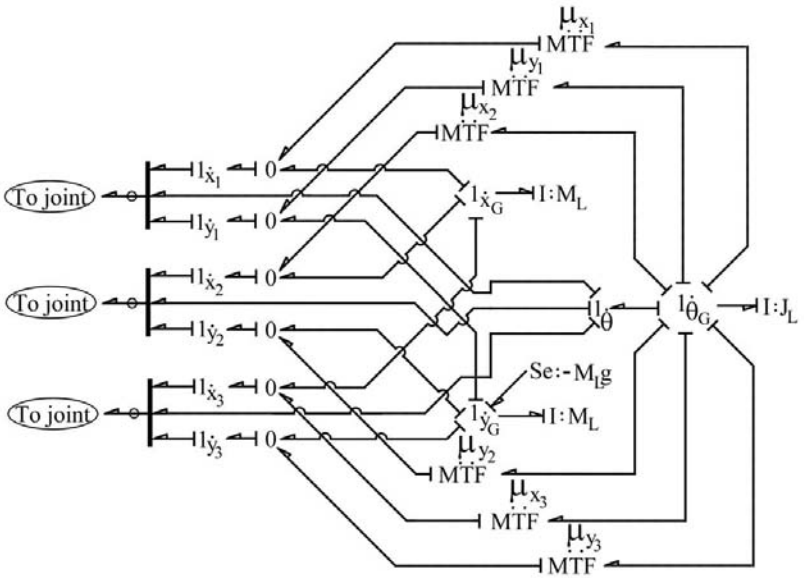

Fig. 2. Its bond graph model

The advantage of bond graph model is that even though we constructed it from kinematic analysis, it automatically takes care of the force and moment balance in the model. When equations are derived from the bond graph model in Fig. 2, one obtains the force and moment balance equations as

$$F_{xG} = \Sigma_i F_{x_i}, \quad F_{yG} = \Sigma_i F_{y_i}, \quad M_{zG} = \Sigma_i(\mu_{x_i} F_{x_i} + \mu_{y_i} F_{y_i}), \tag{4}$$

where F_{x_i} and F_{y_i} are the force components at i^{th} joint, respectively, and F_{xG}, F_{yG} and M_{zG}, represent the resultant forces acting in the x and y directions at the mass center and the resultant moment acting along z-axis at the mass center. These relations are output from the bond graph model. The bond graph model structure, being power conserving, simultaneously represents Eqs. (2) $\sim$ (4) in a compact manner and maintains energetic, dynamic and kinematic consistency of the model.

2.2 Model of the joint component

The joint component is one of the basic components in a mechanism-modelling library. The revolute clearance joint is shown in Fig. 3. Small joint clearance or flexibility (if shrunk-fit) is necessary for ease of assembling the links and also for smooth mobility of the mechanism with reduced friction when a change point configuration is reached. The later is important in case of appreciable thermal expansion or contraction of the links. However, joint clearance also leads to impact forces, rapid wear, rattling and noise[7]. Note that joints without clearance develop some amount of clearance over long use due to normal wear and tear. The normal reaction acts along the attitude line (the line connecting bearing and journal centers in Fig. 3) and frictional forces act perpendicular to attitude line. Various authors have considered various formulations for these forces[1, 7, 26].

The normal and tangential velocities are

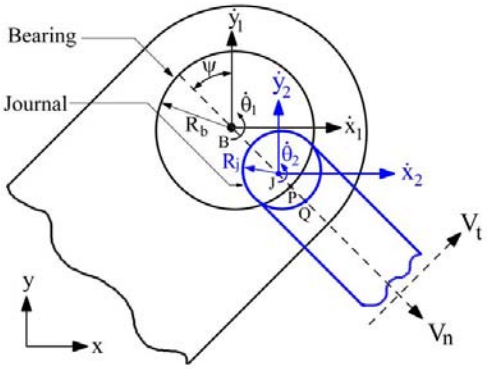

Fig. 3. Bearing and journal of a clearance revolute joint

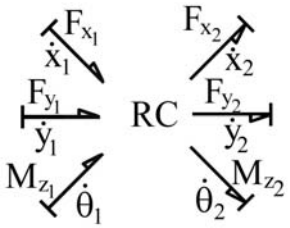

Fig. 4. Bond graph model

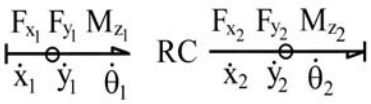

Fig. 5. Its equivalent bond graph

Fig. 6. Schema for rigid links and joint components

$$V_n = (\dot{x}_1 - \dot{x}_2)\sin\psi - (\dot{y}_1 - \dot{y}_2)\cos\psi, \tag{5}$$

$$V_t = (\dot{x}_1 - \dot{x}_2)\cos\psi + (\dot{y}_1 - \dot{y}_2)\sin\psi + (\dot{\theta}_1 R_b - \dot{\theta}_2 R_j), \tag{6}$$

where the variables are defined in Fig. 3. The penetration depth due to impact between the two components is given as $\delta = (BJ - c)$ where the radial clearance $c = R_b - R_j$. Note that δ is taken to be zero when $(BJ - c) < 0$. The normal contact force which is evaluated according to the relation given in [11] as

$$F_n = K\delta^{\alpha} + \left[\frac{3K\delta^{\alpha}(1 - C_e^2)}{4\dot{\delta}^{-}}\right]\dot{\delta} \quad \text{for} \quad \delta > 0, \quad F_n = 0 \quad \text{otherwise.} \tag{7}$$

In Eq. (7) the first term denotes the elastic Hertzian contact force [11, 14] where the stiffness is calculated as $K = 4\sqrt{R_b R_j/(R_b + R_j)}/3(\eta_1 + \eta_2)$, with $\eta_i = (1 - \nu_i^2)/E_i$ are two material parameters[11], ν and E are the Poisson's ratio and Young's modulus, respectively, α is usually taken as 1.5 for contact between metallic bodies, and C_e is the coefficient of restitution used to model impact. The second term in Eq. (7) is due to internal damping of the materials which introduces strain rate dependent damping during impact with $\dot{\delta}^{-}$ being the initial impact velocity and $\dot{\delta}$ is the relative penetration rate. In reference [14], Adams software has been used to model impact forces where the instantaneous damping coefficient has been considered to be a cubic step function of the penetration.

The tangential force is calculated from the modified Coulomb's friction law as follows[7]

$$F_t = -C_f C_d F_n \text{sgn}(V_t), \tag{8}$$

where C_f is coefficient of friction, C_d is dynamic correction coefficient (see [11] for details) and sgn(.) is the signum function. Other forms of dry-friction formulations (e.g., stick-slip[10], honey-drop and Stribeck friction model etc.) may be used here. The formulation given in reference [1] uses Poisson's hypothesis for the definition of the coefficient by first recognizing the correct mode of impact; i.e., sliding, sticking, and reverse sliding. If the clearance between the journal and the bearing is lubricated then fluid-film forces dictate the normal and tangential forces. Bond graph model of journal bearings can be consulted in [21]. However, only dry-friction is considered in the models developed in this article.

The normal and tangential contact forces can be resolved into two components in $x - y$ directions:

$$F_x = F_n \sin\psi + F_t \cos\psi \quad \text{and} \quad F_y = F_n \cos\psi + F_t \sin\psi. \tag{9}$$

The moments acting at the bearing and the journal center due to tangential forces are, respectively,

$$M_b = F_t R_b \quad \text{and} \quad M_j = F_t R_j. \tag{10}$$

The bond graph model of the revolute clearance joint is shown in Fig. 4 and its equivalent bond graph in compact form using vector bonds is shown in Fig. 5. The constitutive relation for the RC-field element (a field element is connected to more than one bonds) is $\bar{e} = \varphi_{RT}(\bar{f}, \int \bar{f} dt, r)$ where r is a set of fixed parameters (geometric and material properties), $\bar{f} = [\dot{x}_1, \dot{y}_1, \dot{\theta}_1, \dot{x}_2, \dot{y}_2, \dot{\theta}_2]^T$ is the vector of generalized flow (velocity) variables, $\bar{e} = [F_{x_1}, F_{y_1}, M_{z_1}, F_{x_2}, F_{y_2}, M_{z_2}]^T$ is the vector of generalized effort variables and $\varphi_{RC}(.)$ function models Eqs. (5) $\sim$ (10). Because the constitutive relation involves both the rate of deformation and deformation to compute the effort (force and moment) variables, the physical phenomenon involved is a combination of dissipation and potential energy storage, which together are represented by a defined bond graph element (RC-field). Note that the attitude angle ψ must be calculated using atan2(.) function such that the quadrant information in not lost during the process.

Three rigid links with joint components are shown in Fig. 6. One of these links is assumed to hold the common journal and is considered to be the reference link. The remaining links form parallel outer races. The clearances between two pairs (link 1 and link 2, and link 1 and link 3) of rigid links are shown in Fig. 7, where r_{cc} is the radius of the clearance circle. The parameter δ_{ij} (where i and j enumerate the links) is the instantaneous distance between the centers of the bolt and the hole in the respective link ends. If no clearance is provided between a pair of links, the corresponding value of r_{cc} is zero. When $\delta_{ij} > r_{cc}$, the interaction force between a pair of links is modelled by Eqs. (7) and (8) and are transformed to inertial frame forces and moments by Eqs. (9) and (10). The bond graph model of many links connected to the common reference link is shown in Fig. 8 where the bold 1-junction is drawn using vector bond graph notation[12] and the dimension of effort and flow variable vectors in each bond is three. This model is an extension of the model given in Fig. 5. The generalized model given in Fig. 8 can be simplified if the joints do not have clearance. Such joints

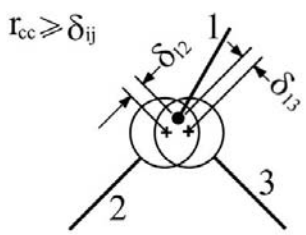

Fig. 7. Its different clearances between two pair of rigid links

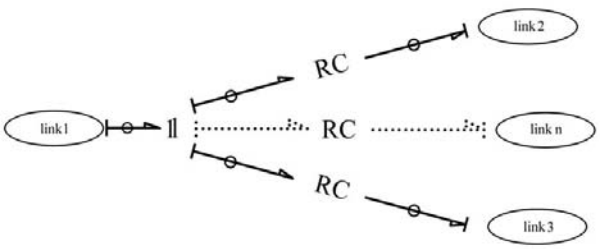

Fig. 8. Its bond graph model

without flexibility are referred to as kinematic joints. However, we will consider joint flexibility in our model. Note that if the joint stiffness is made large in a joint without clearance then the flexible joint behaves as an ideal kinematic joint.

For the flexible joint without clearance, $\delta = BJ$ (from Fig. 3). Furthermore, since $R_b = R_j$, Hertzian contact theory is not applicable because the contact area is more than the characteristic radius of the bodies. The effective stiffness is then considered as K which has to be evaluated experimentally or numerically, e.g., from a finite element model. The damping is proportional to effective stiffness. The proportionality constants between stiffness and damping for various materials are tabulated in reference [6]. Note that without clearance, the stiffness and damping encountered in any radial direction is the same, i.e, the 2×2 stiffness and damping matrices are symmetric and rotationally invariant.

The normal force is then given as

$$F_n = K\delta + \lambda K\dot{\delta}, \tag{11}$$

where λ is the material damping related proportionality constant[6]. The tangential force F_t is still given by Eq. (8).

If dry-friction is neglected and viscous friction is considered (which can be modelled with relative angular velocities) then $F_t = 0$. Consequently, the interaction forces in $x - y$ reference frame between i^{th} link and the reference link (link number 1) are given as

$$\begin{pmatrix} F_x \\ F_y \end{pmatrix} = \begin{bmatrix} K & 0 \\ 0 & K \end{bmatrix} \begin{pmatrix} \int(\dot{x}_i - \dot{x}_1)\mathrm{d}t \\ \int(\dot{y}_i - \dot{y}_1)\mathrm{d}t \end{pmatrix} + \begin{bmatrix} \lambda K & 0 \\ 0 & \lambda K \end{bmatrix} \begin{pmatrix} (\dot{x}_i - \dot{x}_1) \\ (\dot{y}_i - \dot{y}_1) \end{pmatrix}. \tag{12}$$

Separation of the elastic and damping forces and their representation as separate fields (C-field and R-field) yield a simplified bond graph model for joints between several links as shown in Fig. 9. The viscous friction between two links at the joint is modelled by separate R-elements at 0-junctions where relative angular velocities between the links and the reference link are calculated. Likewise, torsional stiffness and damping at the joint may be modelled by 1-C-R structures connected to the 0-junction. If the joint is passive, i.e. actuated, then the motor model with appropriate causalities to apply a torque (effort) may be connected to that 0-junction. The power directions in the bond graph model are set to calculate relative angular velocities at this 0-junction. This also ensures that a motor would apply a forward torque on the driven link and the reverse reactive torque on the driving link.

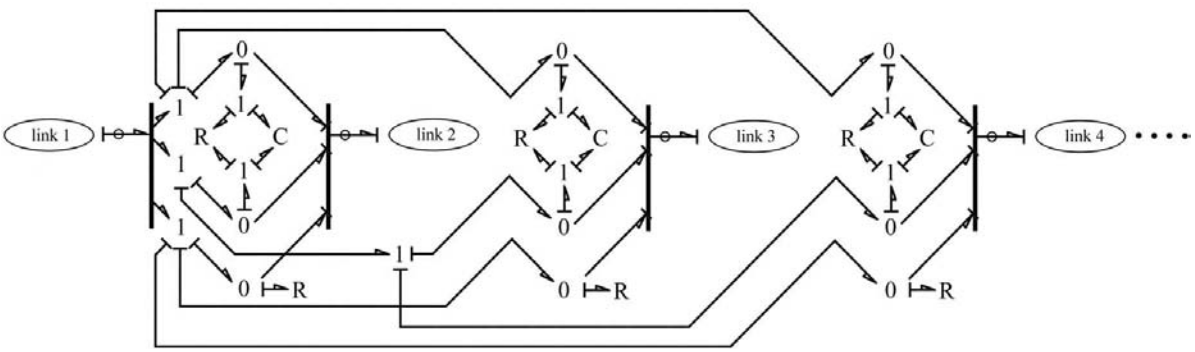

Fig. 9. Bond graph model of an ideal joint component with multiple shear and pin flexibility

When the values of joint stiffness and damping are large, there exists almost same generalized flow in all bonds connected to the joint element from the body components and the impedance coupling tends to become a plain coupling or kinematic joint. Decreasing the value of compliance element can increase the joint flexibility. If the values of damping and compliance parameters are taken to be zero then the connected body components are decoupled. This is how the type of the joint can be changed as per requirement.

2.3 Model of a slider component

The slider is one of the most difficult multibody components which give rise to nonlinear equations of motion. Incorrect modelling of slider components generates improper inertial forces. The schematic view of a plane slider is shown in Fig. 10. The main advantage of a bond graph model is that the radial and tangential forces acting at different points of the model need not be calculated. Simulations supported by theoretical bond graph model of the actual system can determine these dynamic forces.

The velocities of the end points E_c and E_P of the plane slider are expressed as follows:

$$\begin{aligned} \dot{x}_1 &= \dot{x}_{cg} + l_{cg}\dot{\theta}_{cg}\sin\theta_{cg}, \quad \dot{y}_1 = \dot{y}_{cg} - l_{cg}\dot{\theta}_{cg}\cos\theta_{cg}, \\ \dot{x}_2 &= \dot{x}_{pg} - l_{pg}\dot{\theta}_{pg}\sin\theta_{pg}, \quad \dot{y}_2 = \dot{y}_{pg} + l_{pg}\dot{\theta}_{pg}\cos\theta_{pg}. \end{aligned} \tag{13}$$

The rate of change of contemporary length (l) between two points E_c and E_P may be expressed as

$$\dot{l} = \left(\frac{x_1 - x_2}{l}\right)(\dot{x}_1 - \dot{x}_2) + \left(\frac{y_1 - y_2}{l}\right)(\dot{y}_1 - \dot{y}_2). \tag{14}$$

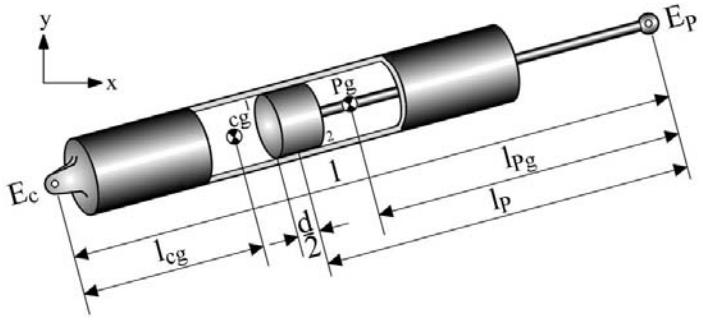

Fig. 10. Schema of a slider model

The normal velocity at the contact point 1 on the cylinder by assuming a thin but long piston is

$$V_{c_1} = -\sin\theta_{cg}\dot{x}_{cg} + \cos\theta_{cg}\dot{y}_{cg} + \left(l - l_p - l_{cg} - \frac{d}{2}\right)\dot{\theta}_{cg}. \tag{15}$$

At the same time, the normal velocity at the contact point 1 on the piston is

$$V_{P_1} = -\sin\theta_{Pg}\dot{x}_{Pg} + \cos\theta_{Pg}\dot{y}_{Pg} - \left(l_p - l_{Pg} + \frac{d}{2}\right)\dot{\theta}_{Pg}. \tag{16}$$

The normal velocities at the contact point 2 on the cylinder and on the piston are, respectively,

$$V_{c_2} = -\sin\theta_{cg}\dot{x}_{cg} + \cos\theta_{cg}\dot{y}_{cg} + \left(l - l_p - l_{cg} + \frac{d}{2}\right)\dot{\theta}_{cg}, \tag{17}$$

$$V_{P_2} = -\sin\theta_{Pg}\dot{x}_{Pg} + \cos\theta_{Pg}\dot{y}_{Pg} - \left(l_p - l_{Pg} - \frac{d}{2}\right)\dot{\theta}_{Pg}. \tag{18}$$

The augmented bond graph model of the system under consideration is shown in Fig. 11 where MTF elements represent modulated transformer[3, 4, 9, 12, 25], i.e., a power conserving transformation element whose modulus is state and/or time dependent. The different multipliers in Eqs. (15) $\sim$ (18) used as MTF moduli in the model are

$$\mu_1 = l_{cg}\sin\theta_{cg}, \quad \mu_2 = -l_{cg}\cos\theta_{cg}, \quad \mu_3 = -\frac{1}{\sin\theta_{cg}}, \quad \mu_4 = \frac{1}{\cos\theta_{cg}},$$
$$\mu_5 = \frac{1}{l - l_P - l_{cg} - d/2}, \quad \mu_6 = \frac{1}{l - l_P - l_{cg} + d/2}, \quad \mu_7 = \frac{x_1 - x_2}{l}, \quad \mu_8 = \frac{y_1 - y_2}{l},$$
$$\mu_9 = -l_{Pg}\sin\theta_{Pg}, \quad \mu_{10} = l_{Pg}\cos\theta_{Pg}, \quad \mu_{11} = -\sin\theta_{Pg}, \quad \mu_{12} = \cos\theta_{Pg},$$
$$\mu_{13} = -\left(l_P - l_{Pg} + \frac{d}{2}\right), \quad \mu_{14} = -\left(l_P - l_{Pg} - \frac{d}{2}\right).$$

In Fig. 11, the sources of efforts indicate the joint forces, labelled 1-junctions represent various velocity points, the masses and the moment of inertias of the slider and rod, respectively, are modelled by the I-elements connected to the 1-junctions representing the velocities of the center of gravity of the two in the inertial frame, the MTF-elements are used to synthesize the constraints. MTF-elements with moduli μ_7 and μ_8 are used to calculate the relative velocity between the piston and the cylinder at a 0-junction and the friction between the piston and the cylinder is modelled by an R-element at that junction. If the cylinder is actuated (e.g., a hydraulic/pneumatic cylinder driven by the pressure difference), the actuating force should be modelled at this 0-junction. Note that if there is dry friction at the piston and cylinder interfaces then the constitutive relation of the R: r_f-element should be modulated by the normal reactions given by 0_1 and 0_2-junctions.

Table 1. The parameter values

$d = 0.4$m	$l = 5$m	$l_{cg} = 1.5$m	$l_P = 0.0$m	$l_{Pg} = 0.0$m	$k_b = 10^5$N/m	$k_p = 10^5$N/m
$r_P = 10^3$N.s/m	$F = 1$N	$J_c = 1$kg.m^2	$J_P = 1$kg.m^2	$M_c = 1$kg	$M_P = 1$kg	$r_f = 0.0$N.s/m

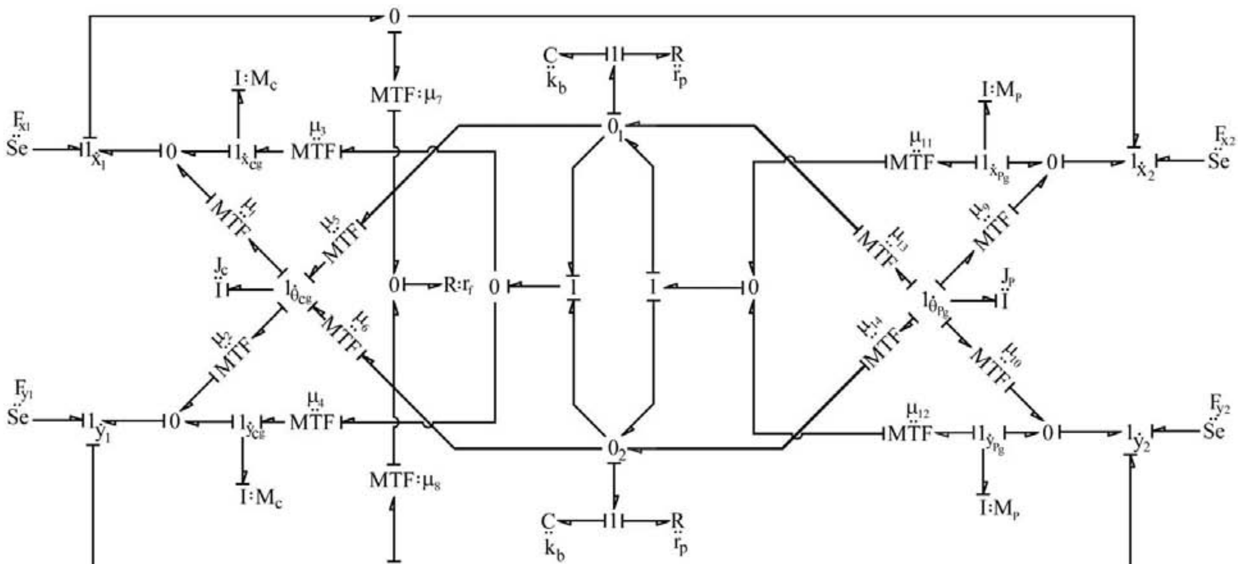

Fig. 11. Bond graph model of the slider component

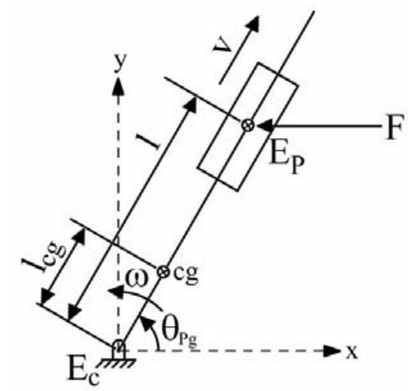

Fig. 12. Schema of Rapson slide

3 Case study-I: Rapson slide

The models developed in the previous sections can be easily extended for three-dimensional systems by including appropriate Euler Junction Structures (EJS)[12, 18] and modified versions of kinematic relations. We consider two benchmark problems in the following sections. In the first case study, we have considered flexible joints without clearance whereas ideal kinematic joints are considered in the second case study.

3.1 Model

In a Rapson slide the slider replaces piston and rod replaces cylinder of the piston-cylinder model given in Fig. 10. The tiller is hinged at the point E_c. The block slides on the rod. We assume that horizontal force acts at the center of the slider and the mechanism lies in a horizontal plane (Fig. 12). The distance of the end point of the piston rod from the combined center of gravity of the piston and rod (Fig. 10) and the distance of the same point from the individual center of gravity of the piston, are set to zero so that the center of gravity of the piston and the end point of the piston rod E_P coincide to each other. With these boundary conditions, the Rapson slide model is equivalent to piston-cylinder model as described before.

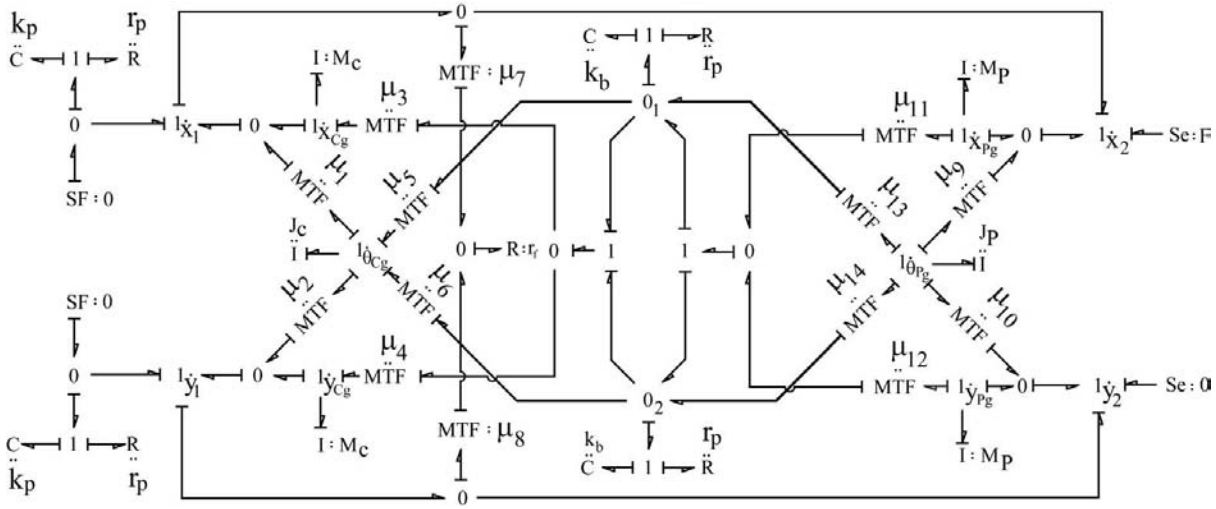

Fig. 13. Bond graph model of Rapson slide

3.2 Bond graph model

The bond graph model of the Rapson slide, shown in Fig. 13, is obtained by slightly modifying the bond graph model of piston-slider model. As the end point of the rod E_c is fixed, two zero flow sources are inserted into the bond graph model. Two coupling capacitors[25] are used with these zero flow sources. Physically, these coupling elements (1-C-R structures) indicate the joint stiffness and damping at the hinge and correlate to interface between two links shown in Fig. 9. The friction at the joint is neglected.

3.3 Simulink model

With reference to the Fig. 12, the forces acting in the radial direction, including centrifugal force, at point E_P are balanced as

$$M_P(\ddot{l} - \dot{\theta}_{Pg}^2 l) + F\cos\theta_{Pg} = 0. \tag{19}$$

The moment due to forces acting in the tangential direction, including Coriolis force, at the point E_P are balanced as

$$J_{eqv}\ddot{\theta}_{Pg} + 2M_P\dot{\theta}_{Pg}l\dot{l} - Fl\sin\theta_{Pg} = 0, \tag{20}$$

where the total equivalent moment of inertia at point E_c is $J_{eqv} = M_P l^2 + J_P + M_c l_{cg}^2 + J_c$. Equations (19-20) are used to construct the Simulink model as shown in Fig. 14. Note that Eqs. (19) and (20) give a very compact model of the Rapson slide mechanism with two degrees of freedom but the contact dynamics and frictional forces between the piston and the cylinder, and joint flexibilities are neglected.

Table 2. The initial conditions

$x_c = 1.2$m	$y_c = 0.9$m	$x_P = 4$m	$y_P = 3$m
$x_1 = 0$m	$y_1 = 0$m	$\theta_c = 0.6435011$rad	$\theta_P = 0.6435011$rad

3.4 Simulation results and validation of the model

The parameter values and the initial conditions are listed in Tabs. 1 and 2 respectively.

We consider that initially a horizontal force of constant magnitude 1 N acts at the center of gravity of the slider in a direction parallel to the reference x-axis. The distance between the points E_c and the center of

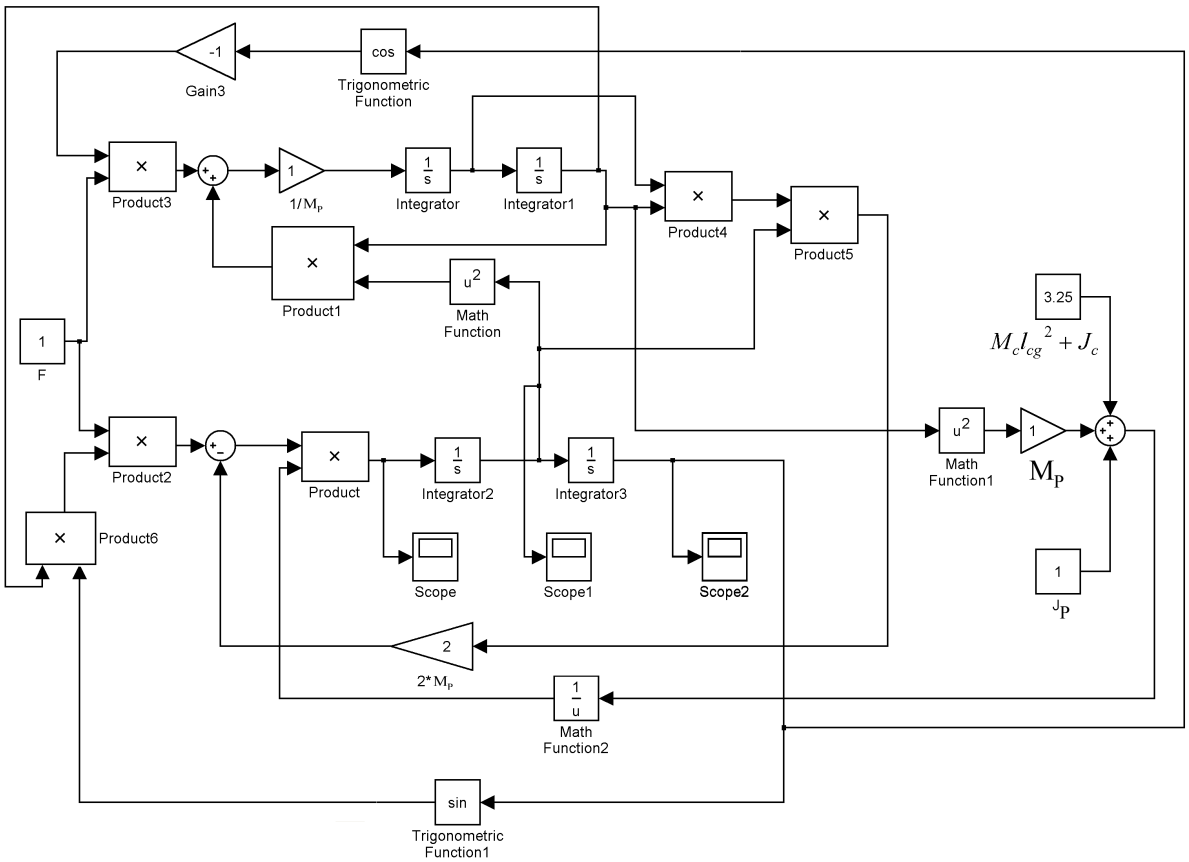

Fig. 14. Simulink model of Rapson slide

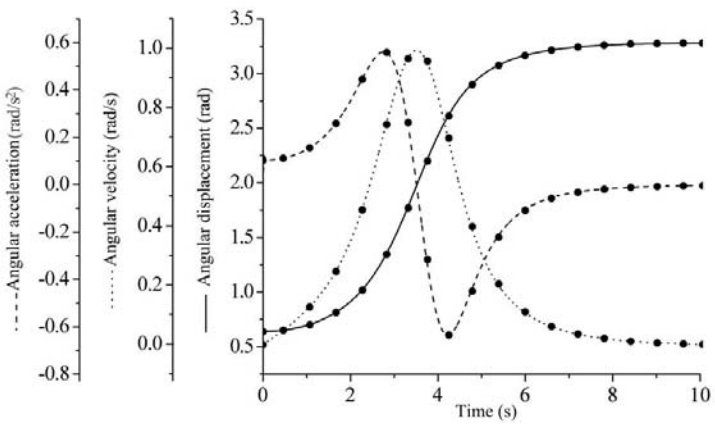

Fig. 15. Angular displacement, velocity and acceleration for the center of the slider. Line indicates Bond graph model, and Scatter points indicate Simulink model

gravity of the piston is 5m. The angular displacement, angular velocity, and the angular acceleration of the slider are shown in Fig. 15 where lines indicate results from the bond graph model and scattered points are results from the Simulink model. The results for the angular velocity and angular acceleration from the two models differ slightly. The difference in angular accelerations of the slider is shown in Fig. 16. These differences are due to the contact forces and joint flexibilities modelled in the bond graph model. The acceleration errors are significant when the joints are initially loaded (near $t = 0s$) and somewhat significant when the rate of acceleration is high, i.e., the motion is jerky[5] (between $t = 2s$ to $t = 6s$). Without consideration of joint flexibility (i.e., when joint stiffness is large), these effects are not visible. Note that integration of acceleration error is almost zero and hence the error between velocity profiles is significantly less. Further integration of

velocity errors yields practically no error in displacement profiles. The joint flexibilities included in the bond graph model yield the transient forces that must be accounted for when designing the linkages for specified strength and fatigue life[5].

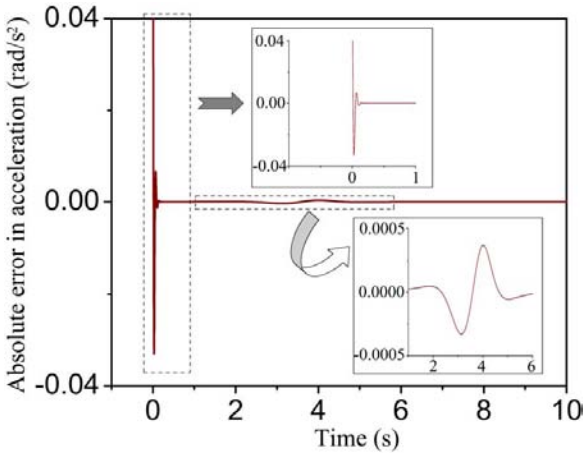

Fig. 16. Absolute error in acceleration

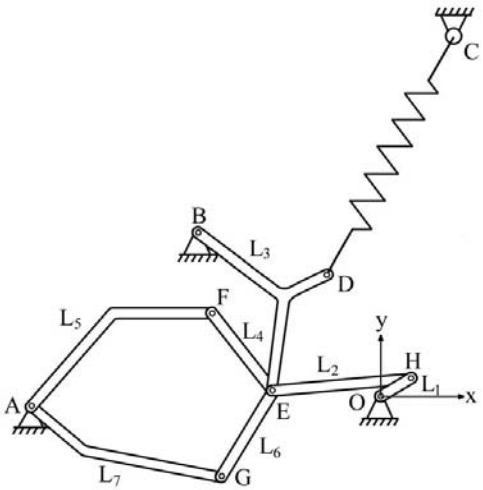

Fig. 17. Seven body mechanism

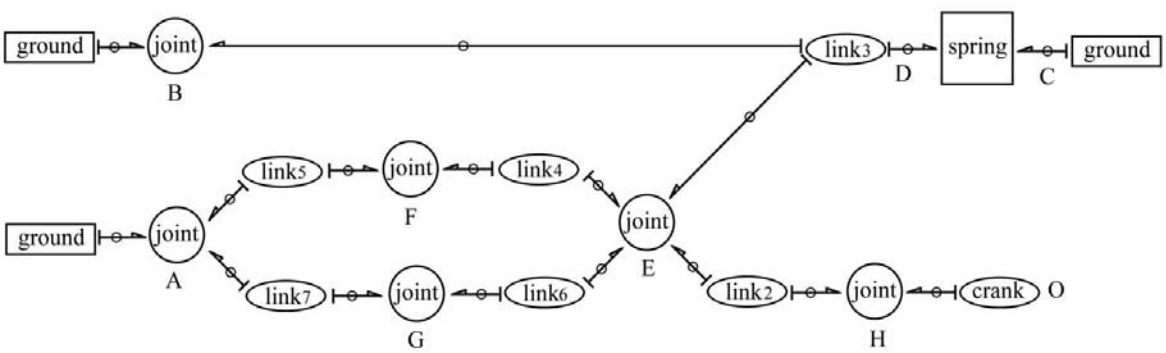

Fig. 18. Its word bond graph

4 Case *II*: Andrews' system

4.1 Model

The seven-body mechanism[23] which is also known as Andrews' system is a benchmark problem adopted in literature on different multibody simulation[16]. It consists of seven irregular shaped bodies, which are connected by frictionless revolute joints as shown in Fig. 17. This mechanism is driven by constant drive torque motor located at point O. The point D of link 3 is connected to the reference frame by a mass less spring. The bond graph model for the rigid bodies $(L_1, L_2, L_4, L_5, L_6, L_7)$ having an arbitrary centroid position was developed in Figs. 1 and 2. Kinematic joints, whose bond graph model was developed in Fig. 3 $\sim$ 5, connect the seven links, spring and ground. The spring is modelled according to Eq. (14) as a two-force member without inertia[18].

The connectivity among different components of the mechanism and with the reference frame at points A, B, C, and O are shown in a word bond graph model in Fig. 18. As the link 5 and link 7 are hinged at the same point A through revolute joints, the grounded joints may be considered together or separately. Links 3, 5 and 7 are connected to the ground through separate revolute joints. Link 1 or the crank is directly connected to the ground. A torque, τ_M, is directly applied to the crankshaft. Bond graph models of the crank and the ground are shown in Fig. 19 and 20.

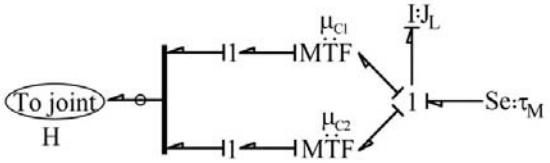

Fig. 19. Bond graph model of (a) crank

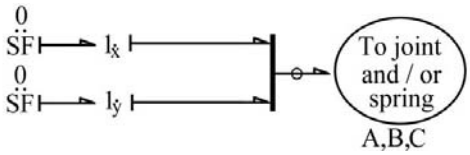

Fig. 20. Bond graph model of (b) ground

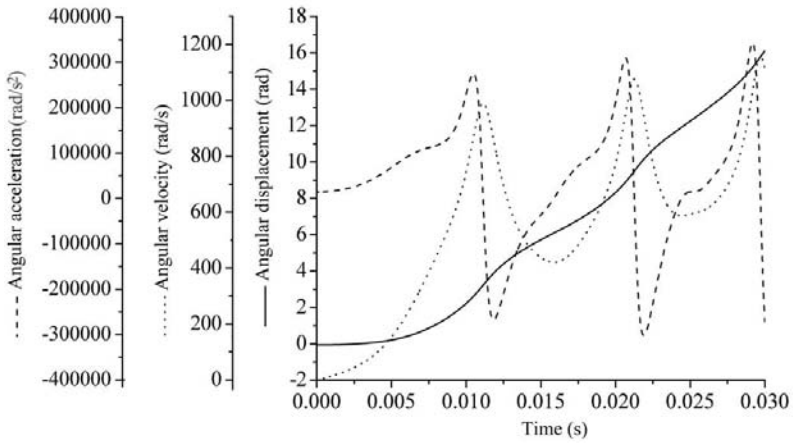

Fig. 21. Angular displacement, velocity and acceleration for the crank

4.2 Simulation results

The geometrical parameters, mass, rotational inertia and initial positions of the fixed points are adopted from reference [23]. Friction-less kinematic joints are considered in reference [23] which is why the large joint stiffnesses and zero coefficient of friction are considered in our model. The constant drive torque τ_M from the motor is 0.033 N.m. The spring coefficient and un-stretched spring length are 4530 N/m and 0.07785 m, respectively. The initial positions of the different points in the mechanism calculated from the geometry specified in [23] are specified as $x_D = -0.010249641$m, $y_D = 0.026190026$m, $x_E = -0.0209593$m, $y_E = 0.0012925$m, $x_F = -0.033996$m, $y_F = 0.01645968$m, $x_G = -0.03163377$m, $y_G = -0.01562066$m, $x_H = 0.00698655$m, $y_H = 0.000433722$m. The joint stiffness and damping were considered as 10^{10} N/m and 10^3 N.s/m, respectively.

The angular displacement, angular velocity, and the angular acceleration of the link 1 or the crank are shown in Fig. 21. Link 1 or the crank completes just one revolution in 16.3 ms. The results for this seven-body mechanism presented in [16] show that the angular displacement of the link1 is below 16 rad after 30 ms whereas our result shows it exceeds 16 rad after 0.029898 s. Our results totally agree with original simulation results presented in [23]. Moreover, the developed bond graph models are modular and it is easier to synthesize models of other planar mechanisms by appropriately assembling various sub-models.

The angular displacement, angular velocity, and the angular acceleration of the link 1 or the crank are shown in Fig. 21. Link 1 or the crank completes just one revolution in 16.3 ms. The results for this seven-body mechanism presented in [16] show that the angular displacement of the link1 is below 16 rad after 30 ms whereas our result shows it exceeds 16 rad after 0.029898 s. Our results totally agree with original simulation results presented in [23]. Moreover, the developed bond graph models are modular and it is easier to synthesize models of other planar mechanisms by appropriately assembling various sub-models.

5 Extension to three-dimensional mechanisms

The planar mechanism models developed so far act as templates on which three-dimensional mechanism models can be built upon. The model structure and composability are retained while extending planar models to three-dimensions.

5.1 Three dimensional prismatic joint

The planar model of prismatic joint can be easily extended to three-dimensional model. The three dimensional cylinder-piston is modelled as a rigid body with twelve degrees of freedom in which the contact between the cylinder and piston impose six constraints. If ideal kinematic constraints are considered then the three dimensional cylinder-piston model has six degrees of freedom. However, we consider constraints allowing local deformations so as to compute normal reactions at contact points and thus to dynamically compute the frictional forces. The rigid body motion is described in body-fixed frame which is attached at the center of mass of the rigid body and aligned with the principal axes. The Newton-Euler equations of the cylinder with attached body fixed axes aligned with the principal axes of inertia are as follows:

$$\sum F_x = M_c\ddot{x}_c + M_c(\dot{z}_c\dot{\theta}_{cy} - \dot{y}_c\dot{\theta}_{cz}), \tag{21}$$

$$\sum F_y = M_c\ddot{y}_c + M_c(\dot{x}_c\dot{\theta}_{cz} - \dot{z}_c\dot{\theta}_{cx}), \tag{22}$$

$$\sum F_z = M_c\ddot{z}_c + M_c(\dot{y}_c\dot{\theta}_{cx} - \dot{x}_c\dot{\theta}_{cy}), \tag{23}$$

$$\sum M_x = J_{cx}\ddot{\theta}_{cx} + \dot{\theta}_{cz}\dot{\theta}_{cy}(J_{cz} - J_{cy}), \tag{24}$$

$$\sum M_y = J_{cy}\ddot{\theta}_{cy} + \dot{\theta}_{cx}\dot{\theta}_{cz}(J_{cx} - J_{cz}), \tag{25}$$

$$\sum M_z = J_{cz}\ddot{\theta}_{cz} + \dot{\theta}_{cy}\dot{\theta}_{cx}(J_{cy} - J_{cx}), \tag{26}$$

where F_x, F_y and F_z are external forces acting in body-fixed x, y and z directions, respectively, M_x, M_y and M_z are external moments acting in body-fixed x, y and z directions, respectively, M_c is the mass of the cylinder, J_{cx}, J_{cy} and J_{cz} are the moment of inertias about principal axes, $\dot{x}_c$, $\dot{y}_c$ and $\dot{z}_c$ are velocities of the mass center in the body-fixed frame, $\ddot{x}_c$, $\ddot{y}_c$ and $\ddot{z}_c$ are accelerations of the mass center in the body-fixed frame, $\dot{\theta}_{cx}$, $\dot{\theta}_{cy}$ and $\dot{\theta}_{cz}$ are angular velocities of the mass center in the body-fixed frame, and $\ddot{\theta}_{cx}$, $\ddot{\theta}_{cy}$ and $\ddot{\theta}_{cz}$ are angular accelerations of the mass center in the body-fixed frame.

In the bond graph model of the three-dimensional prismatic joint shown in Fig. 22, the inertias are coupled by a pair of gyrator rings (Euler junction structures) [12, 18], one for translational and the other for rotational velocities, according to Eqs. (21) $\sim$ (26). They introduce six degrees of freedom. Likewise, six more degrees of freedom are considered for the piston and the piston rod. They are represented by another pair of gyrator rings and the variables used in that part of the model are represented by similar nomenclature where subscript 'p' used in place of 'c' to indicate that they are associated with the piston.

The co-ordinate transformation (CTF) blocks in Fig. 22 are required to transform body fixed velocities to the inertial velocities. The rate of change of contemporary length (l) between cylinder end and the piston is expressed as

$$\dot{l} = \left(\frac{X_1 - X_2}{l}\right)(\dot{X}_1 - \dot{X}_2) + \left(\frac{Y_1 - Y_2}{l}\right)(\dot{Y}_1 - \dot{Y}_2) + \left(\frac{Z_1 - Z_2}{l}\right)(\dot{Z}_1 - \dot{Z}_2), \tag{27}$$

where (X_1, Y_1, Z_1) represents the coordinates of the cylinder end point in the inertial frame and (X_2, Y_2, Z_2) represents the coordinates of the piston end point in the inertial frame. The position of the cylinder end point with respect to the body-fixed frame at the mass center is given as (x_1, y_1, z_1) and that for the piston end point with respect its body-fixed frame is given as (x_2, y_2, z_2). The velocities of these points are represented in the bond graph model at 1-junctions with appropriate suffixes. The linear and angular velocities of the mass centers of the cylinder and piston are used to compute velocities of the end points in respective body-fixed frames and then they are transformed to inertial velocities to implement constraints in the inertial frame, i.e., Eq. (27) and external forces (joint forces) acting at the end points of the cylinder and the piston. The end point joint forces are inputs to the model given at ports ① and ②.

MTF-elements with moduli μ_x, μ_y and μ_z are used to calculate the relative sliding velocity between the piston and the cylinder at a 0-junction and the friction between the piston and the cylinder is modelled by an R-element at that junction. A set of transformers with moduli c_1 to c_4 and p_1 to p_4 are determined from kinematic analysis to compute the velocities of the contact points on the cylinder and the piston in respective body-fixed

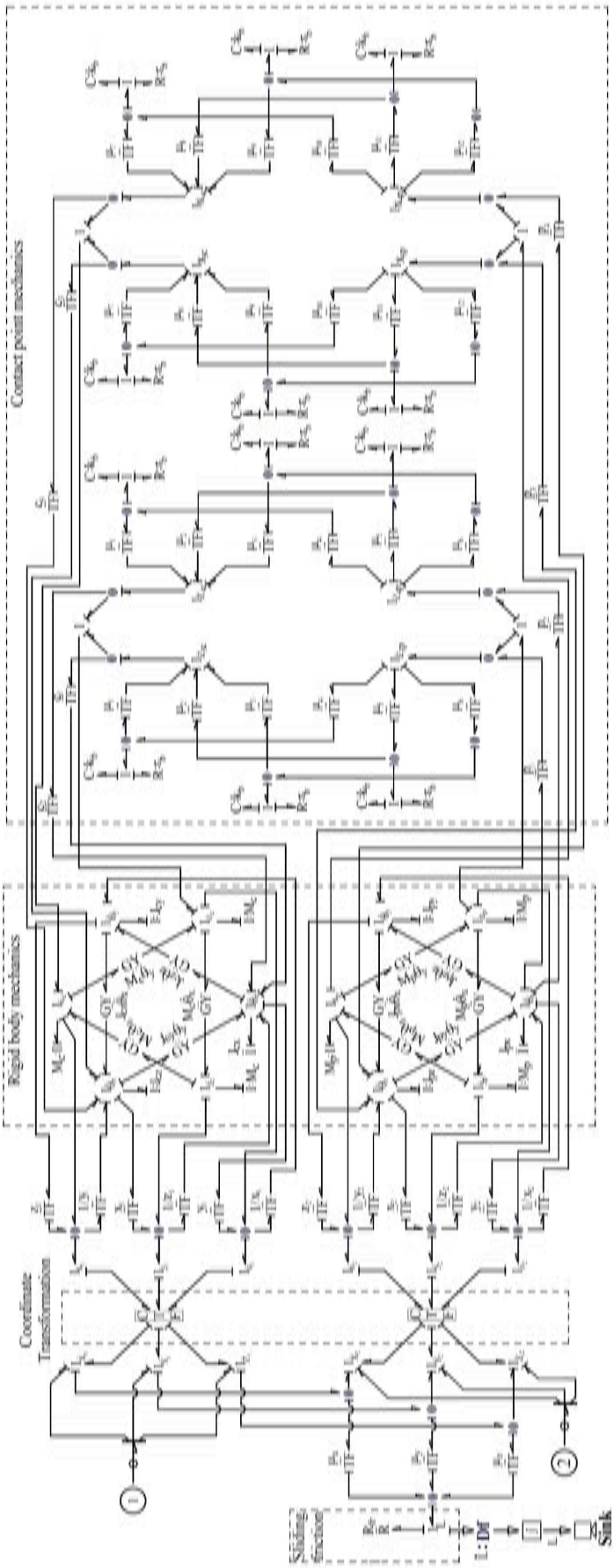

Fig. 22. Bond graph model of three dimensional prismatic joint

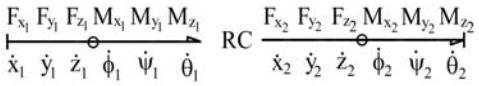

Fig. 23. Bond graph model of three dimensional revolute joint

frames. These body-fixed velocities are transformed to inertial velocities (through a set of transformers with moduli μ_1 to μ_{12}) and are then implicitly constrained. The normal velocity at the contact point on the cylinder is made equal to normal velocity at the contact point on the piston by providing higher values of contact stiffness and damping parameters, k_b and r_b, respectively. In comparison to other stiffness at the contact point, the bending stiffness of the piston rod is lowest and hence k_b and r_b and are approximated to represent the bending stiffness and damping of the piston rod.

5.2 Three dimensional revolute joint

The bond graph model of three-dimensional revolute clearance joint in compact form using vector bonds is shown in Fig. 23. The constitutive relation for the RC-field element (a field element is connected to more than one bonds) is $\bar{e} = \varphi_{RC}(\bar{f}, \int \bar{f}\mathrm{d}t)$ where r is a set of fixed parameters (geometric and material properties), $\bar{f} = [\dot{x}_1, \dot{y}_1, \dot{z}_1, \dot{\phi}_1, \dot{\psi}_1, \dot{\theta}_1, \dot{x}_2, \dot{y}_2, \dot{z}_2, \dot{\phi}_2, \dot{\psi}_2, \dot{\theta}_2,]^T$ is the vector of generalized flow (velocity) variables, $\bar{e} = [F_{x_1}, F_{y_1}, F_{z_1}, M_{x_1}, M_{y_1}, M_{z_1}, F_{x_2}, F_{y_2}, F_{z_2}, M_{x_2}, M_{y_2}, M_{z_2}]^T$ is the vector of generalized effort variables and $\varphi_{RC}(.)$ function models the constitutive relation of the joint.

6 Conclusions

Bond graph modelling of planar mechanical systems consisting of rigid body components and revolute joints was considered in this paper. Thereafter, the bond graph model of a joint with looseness was developed to model the impact forces due to joint clearance. The main objective of this article was to develop composable sub-models of a planar mechanical library which can be easily integrated to create the model of a complex mechanism and mass distribution in prismatic or slider joints are developed. A generalized model of a slider component with two moving contact points was developed from the first principles. We have developed the models in such a way that by varying suitable geometrical parameter values, various mechanism configurations can be represented. Two separate case studies, a Rapson slide and a seven-body mechanism, are considered to validate the developed models. It has been shown that the planar joint models can be extended easily to form three-dimensional joint models.

This paper does not merely explain some particular mechanism, but forms a basis for development of a mechanism library by using bond graph models. The models developed in the article are modular, i.e., they can be easily interfaced with other models and extended by adding other dynamical parts. Mechanisms are often used with other devices, e.g., the slider-crank mechanism connects the IC engine to the fluid coupling of the automatic transmission system of a vehicle. The multi-energy domain representation through bond graph modelling allows for integration of electrical, hydraulic/ pneumatic and thermal domains, etc. into the model.

References

[1] S. Ahmed, H. Lankarani, M. Pereira, Frictional impact analysis in open-loop multibody mechanical systems. *Journal of Mechanical Design, Transactions of the ASME*, 1999, **121**(1): 119–127.

[2] J. Baumgarte. Stabilization of constraints and integrals of motion in dynamical systems. *Computer Methods in Applied Mechanics and Engineering*, 1972, **1**: 1–16.

[3] W. Borutzky. *Bond Graphs—A Methodology for Modelling Multidisciplinary Dynamic Systems*. SCS Publishing House, San Diego, 2004.

[4] G. Dauphin-Tanguy. *Les Bond Graphs*. Hermes Science Europe Ltd, Paris, 2000.

[5] S. Erkaya, I. Uzmay. Investigation on effect of joint clearance on dynamics of four-bar mechanism. *Nonlinear Dynamics*, 2009, **58**(1-2): 179–198.

[6] A. Filippov. *Vibrations of Mechanical systems*. National Lending Library for Science and Technology, Boston Spa, Yorkshire, England, 1971.
[7] P. Flores. Modeling and simulation of wear in revolute clearance joints in multibody systems. *Mechanism and Machine Theory*, 2009, **44**(6): 1211–1222.
[8] P. Flores, J. Ambrosio, et al. *Kinematics and Dynamics of Multibody Systems with imperfect joints: Models and case studies*. Springer, Berlin/Heidelberg, 2008.
[9] P. Gawthrop, L. Smith. *Metamodelling: Bond Graphs and Dynamic Systems*. Prentice Hall, 1996.
[10] D. Karnopp. Computer simulation of stick-slip friction in mechanical dynamic systems. *Journal of Dynamic Systems, Measurement and Control, Transactions of the ASME*, 1985, **107**(1): 100–103.
[11] D. Karnopp, D. Margolis. Analysis and simulation of planar mechanism systems using bond graphs. *Journal of Mechanical Design*, 1979, **101**(2): 187–191.
[12] D. Karnopp, D. Margolis, R. Rosenberg. *System Dynamics: Modeling and Simulation of Mechatronic Systems*. John Wiley & Sons Incorporated, 2006.
[13] R. Kübler, W. Schiehlen. Modular simulation in multibody system dynamics. *Multibody System Dynamic*, 2000, **4**(2-3): 107–127.
[14] I. Khemili, L. Romdhane. Dynamic analysis of a flexible slider-crank mechanism with clearance. *European Journal of Mechanics, A/Solids*, 2008, **27**(5): 882–898.
[15] W. Marquis-favre, E. Bideaux, S. Scavarda. A planar mechanical library in the amesim simulation software. part i: Formulation of dynamics equations. *Simulation Modelling Practice and Theory*, 2006, **14**(1): 25–46.
[16] W. Marquis-favre, E. Bideaux, S. Scavarda. A planar mechanical library in the amesim simulation software. part ii: Library composition and illustrative example. *Simulation Modelling Practice and Theory*, 2006, **14**(2): 95–111.
[17] J. McPhee. On the use of linear graph theory in multibody system dynamics. *Nonlinear Dynamics*, 1996, **9**(1-2): 73–90.
[18] A. Mukherjee, R. Karmakar, A. Samantaray. *Bond Graph in Modeling, Simulation and fault Identification*. CRC Press, Florida, 2006.
[19] M. Otter, H. Elmqvist, F. Cellier. Modeling of multibody systems with the object-oriented modeling language dymola. *Nonlinear Dynamics*, 1996, **9**(1): 91–112.
[20] A. Sagirli, M. Bogoclu, V. Omurlu. Modeling the dynamics and kinematics of a telescopic rotary crane by the bond graph method (part i). *Nonlinear Dynamics*, 2003, **33**: 337–351.
[21] A. Samantaray, R. Bhattacharyya, A. Mukherjee. An investigation into the physics behind the stabilizing effects of two-phase lubricants in journal bearings. *Journal Vibration and Control*, 2006, **12**(4): 425–442.
[22] S. Sandhu, J. McPhee. Partitioned dynamic simulation of multibody systems. *Journal of Computational and Nonlinear Dynamics*, 2010, **5**(3): 1–7.
[23] W. Schiehlen. *Multibody Systems Handbook*. Springer Verlag, Berlin, 1990.
[24] W. Schiehlen. Multibody system dynamics: Roots and perspectives. *Multibody System Dynamics*, 1997, **1**: 149–188.
[25] J. Thoma, B. Bouamama. *Modelling and Simulation in Thermal and Chemical Engineering*. Springer-Verlag, New York, 2000.
[26] Q. Tian, Y. Zhang, et al. Simulation of planar flexible multibody systems with clearance and lubricated revolute joints. *Nonlinear Dynamics*, 2010, **60**: 489–511.